Naval Research Laboratory

Washington, DC 20375-5320

Synthetic Aperture Ladar (SAL): Fundamental Theory, Design Equations for a Satellite System, and Laboratory Demonstration

Robert L. Lucke
Lee J Rickard

Radio/IR/Optical Sensors Branch
Remote Sensing Division

Mark Bashkansky

Optical Physics Branch
Optical Sciences Division

Jonh Reintjes

Optical Sciences Division

Eric E. Funk

Photonics Technology Branch
Optical Sciences Division

December 26, 2002

REPORT DOCUMENTATION PAGE

Form Approved
OMB No. 0704-0188

1. REPORT DATE *(DD-MM-YYYY)*	**2. REPORT TYPE**	**3. DATES COVERED** *(From - To)*
26-12-2002	Formal	May 2001 to December 2002

4. TITLE AND SUBTITLE

Synthetic Aperture Ladar (SAL): Fundamental Theory, Design Equations for a Satellite System, and Laboratory Demonstration

5a. CONTRACT NUMBER

5b. GRANT NUMBER

5c. PROGRAM ELEMENT NUMBER
0603011F

6. AUTHOR(S)

Robert L. Lucke, Lee J Rickard, Mark Bashkansky, John Reintjes, and Eric E. Funk

5d. PROJECT NUMBER
RDTEAF

5e. TASK NUMBER

5f. WORK UNIT NUMBER
72-8143-02

7. PERFORMING ORGANIZATION NAME(S) AND ADDRESS(ES)

Naval Research Laboratory
Washington, DC 20375-5320

8. PERFORMING ORGANIZATION REPORT NUMBER

NRL/FR/7218--02-10,051

9. SPONSORING / MONITORING AGENCY NAME(S) AND ADDRESS(ES)

U.S. Air Force
P.O. Box 46355
Washington, DC 20050-6335

10. SPONSOR / MONITOR'S ACRONYM(S)

11. SPONSOR / MONITOR'S REPORT NUMBER(S)

12. DISTRIBUTION / AVAILABILITY STATEMENT

Approved for public release; distribution is unlimited.

13. SUPPLEMENTARY NOTES

14. ABSTRACT

The carrier-to-noise ratio (CNR) resulting from phase-sensitive heterodyne detection in a photon-limited synthetic aperture ladar (SAL) is developed, propagated through synthetic aperture signal processing, and combined with speckle to give the signal-to-noise ratio (SNR) of the resulting image. CNR and SNR are defined in such a way as to be familiar to the optical imaging community. Design equations are presented to allow quick assessment of the hardware parameters required for a notional system, most notably optical aperture sizes and the laser's power, chirp, and pulse rate capabilities. Some tutorial information on phase-sensitive heterodyne detection and synthetic aperture image formation is provided. The first two-dimensional synthetic aperture imaging in the optical domain is demonstrated in a laboratory setting.

15. SUBJECT TERMS

Synthetic aperture ladar (SAL)

16. SECURITY CLASSIFICATION OF:			**17. LIMITATION OF ABSTRACT**	**18. NUMBER OF PAGES**	**19a. NAME OF RESPONSIBLE PERSON** Robert Lucke
a. REPORT	**b. ABSTRACT**	**c. THIS PAGE**	SAR	31	**19b. TELEPHONE NUMBER** *(include area code)* 202-767-2749
Unclassified	Unclassified	Unclassified			

Standard Form 298 (Rev. 8-98)
Prescribed by ANSI Std. Z39.18

CONTENTS

SYNTHETIC APERTURE LADAR: FUNDAMENTAL THEORY, DESIGN EQUATIONS FOR A SATELLITE SYSTEM, AND LABORATORY DEMONSTRATION

1. INTRODUCTION

A synthetic aperture ladar (SAL) could provide dramatic improvements in either resolution or, compared to synthetic aperture radar (SAR), the time needed to record an image, or both. The reduced imaging time results from the shorter time needed by the platform to traverse the synthetic aperture (SA) that produces the same resolution with a shorter wavelength. When the observation range reaches a thousand kilometers or more, no other method of imaging can offer centimeter-class resolution with a real aperture size no larger than a few meters. Additionally, because SAL is an active sensing method, it is not restricted to daylight operation. This report investigates one of the few limits on SAL that is of a theoretical nature: the limit imposed by photon statistics (a limit that is not relevant to SAR). A criterion is developed for the number of photons that is needed for each resolution element of an image, and design equations are given to evaluate a proposed design with respect to this criterion. The engineering problems of implementing SAL are less easily dealt with. The more prominent are indicated below, but their actual means of solution are resolutely ignored in this report. A brief treatment of the effects of propagation through the atmosphere is given in Section 2.7. It indicates that high-resolution SAL imaging from orbit is possible, but much more work needs to be done on this topic, because the atmosphere can degrade beam quality substantially at visible and infrared wavelengths.

Previous work on SAL [1,2 and references cited therein] has not considered the implications of photon statistics and, in the laboratory, has usually used fixed-frequency CW lasers and measured Doppler shifts from moving targets to create an image. The approach to SAL analyzed here [3] is the SAR technique of transmitting a series of FM-chirped pulses, heterodyning the return signal with a similarly chirped local oscillator (LO), isolating a single range resolution element as a narrow-frequency subband of the detector's output (a process called deramping, described in Section 10.1 of Curlander and McDonough [4] or Section 1.3 of Jakowatz et al. [5]), and match-filtering data from this subband to pick out an azimuth resolution element by its phase history. As discussed in Section 3, this technique has recently been demonstrated at 1.55 μ in a laboratory-scale experiment [6], though not yet in the photon-limited regime. This report examines the effects of photon statistics and of speckle on imagery from a space-based system. We are motivated in part by a desire to bridge the gap between the heterodyne detection and optical imaging communities, so the development will include some relevant tutorial information, but we assume a reasonable degree of familiarity with the physical principles of heterodyne detection lidar (see, for example, Shapiro et al. [7] and references cited therein) and SA image formation [4,5]. Park and Shapiro [8] discuss a similar system (their Doppler pulse compression is the equivalent of the phase history matched filter described here), but they emphasize short-range (< 100 km), air-based operation and do not consider photon statistics or speckle. Kyle [9] proposes a SAL system that transmits a coded pulse stream, rather than an FM chirp, to resolve range. The method is theoretically sound, but requires very fast modulation of the laser and wideband detectors. Kyle [9] evaluates his system in much the same way as presented here in Section 2.5, but drastically overstates the signal-to-noise ratio (SNR) of his illustrative example. Aleksoff et al. [10] show the full potential of SA imaging with a laboratory

demonstration of a 3-D SAL, but the method requires 2-D motion of the platform and is therefore unsuitable to the imaging problem considered here.

   The system modeled here is a scan-mode SAL that transmits a beam with a ground footprint having an instantaneous diameter that contains M pixels. As the motion of the sensor's platform sweeps the beam along the ground, M pulses, each of time duration τ_{pul}, are transmitted during the dwell time, τ_{dw}, the time a single pixel remains illuminated. The minimum detectable frequency difference in the heterodyne signal is $\delta f = 1/\tau_{pul}$, and this, combined with the chirp rate, determines the minimum resolvable range element. Azimuthal SA processing requires measuring both the amplitude and phase of the light scattered from the scene, and at optical frequencies this can be done only with heterodyne detection. The fact that phase must be measured separates SAL from conventional optical heterodyne systems, which are used as sensitive detectors of narrow-band light, but measure only the number of photons received, not their phase. For this reason, SAL necessitates a more thorough treatment of shot noise than is normally required.

   For a photon-limited direct detector, the number of signal photons detected in a single measurement is known, but the same cannot be said for a photon-limited heterodyne detector. Because of shot noise from the LO, it is impossible to conclude that a particular number of signal photons was detected in a measurement. Consequently, the value of n, the number of signal photons inferred from the heterodyne measurement, is not restricted to integral values and is treated as a continuous variable when its probability density function (PDF) is considered. The PDF is needed to calculate the carrier-to-noise ratio (CNR) and, combined with speckle, the SNR. CNR is an unfamiliar term in normal, direct-detection optical imaging: it means SNR before the effect of speckle is included. The definition of CNR normally used for heterodyne detection is a legacy of its RF origin and leads to a photon-limited CNR proportional to the number of signal photons instead of the square root of this number. The photon-limited CNR for SAL will be defined to be proportional to the square root of the number of signal photons, a definition more familiar to the optical imaging community. CNR and SNR for SAL will be compared to those for a direct detection system that detects the same number of photons from one polarization of the light returned from a coherently illuminated scene (recall that scattering from ordinary surfaces randomizes polarization). In other words, SAL will be compared to a direct-detection system with a polarizer in it. CNRs and SNRs can always be improved by a factor of $\sqrt{2}$ by measuring both polarizations, but this is far easier to do with a direct-detection system (just remove the polarizer!) than with a heterodyne system, for which a beamsplitter and an additional detection channel must be added. Speckle limits the SNR of single-look imagery to, at most, unity for SAL, just as it does for SAR or for direct detection. Fortunately, the limit can be closely approached when only a few photons per pixel are received.

   Section 2.1 describes phase-sensitive heterodyne detection, with emphasis on the fact that signal and noise are complex numbers in Fourier space. Section 2.2 derives the appropriate CNR for an imaging system and compares it to the traditional RF definition, Section 2.3 propagates signal and noise through synthetic aperture processing, and Section 2.4 combines the result with speckle to produce the SNR of the SAL image. Section 2.5 presents design equations, with emphasis on the specifications of the laser. Section 2.6 describes the effect of a moving object in the scene and Section 2.7 compares the angle swept out by the satellite with respect to the ground observation point to the isoplanatic angle of the atmosphere.

2. FUNDAMENTAL THEORY AND DESIGN EQUATIONS

2.1 Phase-Sensitive Heterodyne Detection

   A light wave with frequency f and phase ϕ is described by $E\exp(2\pi ift + i\phi)$ with E real and non-negative, and the units of E are chosen so that power is related to the electric field by

$$P = \int_{area} \frac{1}{2}|E \exp(2\pi ift + i\phi)|^2 \, dxdy \equiv \frac{1}{2} A_d \overline{E}^2 \quad , \tag{1}$$

where the integral is over the area, A_d, of the detector, E may be, and usually is, a function of position on the detector, and $\overline{E}$ is the appropriate average. To relate $\overline{E}$ to N, the average number of photons in pulse time τ_{pul} (N need not be an integer), we write $P = h\nu N/\tau_{pul}$, where $h = 6.63 \times 10^{-34}$ joule-sec is Planck's constant and ν is the frequency of the light, to find that

$$\overline{E} = \sqrt{\frac{2h\nu N}{A_d \tau_{pul}}} \quad . \tag{2}$$

An FM-chirped waveform is generated by linearly sweeping the laser's frequency over a range Δf_{ch} during the pulse time, so the field of the LO is $E_L \exp[2\pi i(f_0 + \frac{1}{2}\dot{f}\, t)t]$ where $\dot{f} = \Delta f_{ch}/\tau_{pul}$ is the chirp rate. The field of the signal from a single range resolution element, being displaced in time by some amount Δt and having an arbitrary phase ϕ_{S0} with respect to the LO, is $E_S \exp\{2\pi i[f_0 + \frac{1}{2}\dot{f}\,(t + \Delta t)](t + \Delta t) + i\phi_{S0}\}$. In heterodyne detection the fields are combined on the detector to yield a detector output current given by

$$\begin{aligned} I_d &= \eta_d \frac{q_e}{h\nu} \int_{area} \frac{1}{2}\left|E_L \exp[2\pi i(f_0 + \frac{1}{2}\dot{f}t)t] + E_S \exp\{2\pi i[f_0 + \frac{1}{2}\dot{f}(t + \Delta t)](t + \Delta t) + i\phi_{S0}\}\right|^2 dxdy \\ &= \eta_d \frac{q_e}{h\nu}\left[\frac{1}{2} A_d \overline{E}_L^2 + \frac{1}{2} A_d \overline{E}_S^2 + A_d \sqrt{\eta_h}\, \overline{E}_L \overline{E}_S \cos(2\pi\Delta ft + \phi_S)\right] \\ &= q_e \eta_d \frac{N_L + N_S}{\tau_{pul}} + 2q_e \eta_d \frac{\sqrt{\eta_h N_L N_S}}{\tau_{pul}} \cos(2\pi\Delta ft + \phi_S) \quad , \end{aligned} \tag{3}$$

where η_d is the detector's quantum efficiency, assumed constant across the detector, q_e is the charge of an electron, $q_e/h\nu$ performs the detector's transducer function of replacing $h\nu$ by q_e, η_h is the heterodyne mixing efficiency[11], $\Delta f = \dot{f}\,\Delta t$ is the beat frequency, $\phi_S = \phi_{S0} + 2\pi(f_0\Delta t + \frac{1}{2}\dot{f}\,\Delta t^2)$, and Eq. (2) has been used. The first term in the third equality of Eq. (3), when multiplied by τ_{pul}/q_e, is the total number of electrons generated (= photons detected). The second term identifies the range element in question by its beat frequency Δf. A different range element yields a different Δf, a relation that will be stated precisely in Section 2.5. Equation (3) is most easily understood from the point of view of the semiclassical theory [12], that the field itself may be treated classically, that is, without intrinsic fluctuations. Fluctuations in the number of photons detected results from a stochastic interaction between the electromagnetic field and the detector: shot noise, which is treated below.

Equation (3) is written for a single range resolution element. In the detector's actual output, there are M such terms, having M different frequencies, one for each range resolution element in the footprint. In order to satisfy the Nyquist criterion, the detector's output is digitized with (at least) $2M$ samples over the time τ_{pul}, and the value of the Δf component of the discrete Fourier transform (DFT) of these samples is

$$\begin{aligned} D(\Delta f) &= \frac{\tau_{pul}}{2M} \sum_{m=0}^{2M-1} 2q_e \eta_d \frac{\sqrt{\eta_h N_L N_S}}{\tau_{pul}} \cos(2\pi\Delta ft_m + \phi_S) \exp(-2\pi i\Delta ft_m) \\ &= q_e \eta_d \sqrt{\eta_h N_L N_S} \exp(i\phi_S) \quad , \end{aligned} \tag{4}$$

where $\tau_{pul}/2M$ normalizes the DFT so that its DC component is the total charge generated and $t_m = m\tau_{pul}/2M$ is the time of the mth sample. $D(\Delta f)$ is divided by $q_e\eta_d(\eta_h N_L)^{1/2}$ to obtain the desired value, $D'(\Delta f) = N_S^{1/2}\exp(i\phi_S)$, that is needed for SA processing. It is a basic property of the DFT that the separation between the DFT's discrete frequency components is $\delta f = 1/\tau_{pul}$, so D' is the signal over bandwidth δf (i.e., from one range resolution element) at a frequency displaced by Δf from the frequency of the LO.

In the photon-limited regime, the dominant source of noise is shot noise from the total number of photons detected, which is $\eta_d(N_L + N_S)$. Normally $N_L \gg N_S$, and that approximation will be used here. $N_L \gg 1$ always. As shown in Appendix A, the noise at any frequency is described by a 2-D Gaussian distribution [Eq. (A1) with $s = 0$] with, replacing N in Eq. (A5) by $N_L + N_S$, $\sigma^2 = q_e^2\eta_d(N_L + N_S)/2 \approx q_e^2\eta_d N_L/2$. This is the noise on the signal D. If a random variable is divided by a constant to obtain a new random variable, the variance of the old variable must be divided by the square of the constant to obtain the variance of the new one. Since D is divided by $q_e\eta_d(\eta_h N_L)^{1/2}$ to obtain the desired value, D', σ^2 must be divided by the square of this factor, $(q_e\eta_d)^2\eta_h N_L$, to obtain

$$\sigma'^2 = \frac{1}{2\eta_d\eta_h}. \tag{5}$$

That is, the PDF of the random variable D' plus noise is a 2-D Gaussian centered on $N_S^{1/2}\exp(i\phi_S)$ with width given by σ'^2, as illustrated schematically in Fig. 1. With signal and noise now specified, we are ready to describe SA processing and see how noise propagates through it, but it is instructive to pause at this point to examine the CNR and the number and phase uncertainties of heterodyne detection.

2.2 Carrier-to-Noise Ratio

As stated above, CNR is SNR before speckle is taken into account, so the results of this section apply to a coherent-light sensor that makes repeated measurements without changing the part of the speckle field it samples. In optical imaging, the normal definition of SNR or CNR is the ratio of the magnitude of a signal to the standard deviation (square root of the variance) of the signal's estimator. For photon-counting direct detection, the number of detected photons, n, follows Poisson statistics with $\langle n \rangle = \eta_d N_S$. Now, n must be divided by η_d to obtain an estimate of the signal: $\langle n/\eta_d \rangle = N_S$. For the Poisson distribution the variance is equal to the mean, that is, $\mathrm{Var}(n) = \langle n \rangle = \eta_d N_S$, which must be divided by η_d^2 to obtain N_S/η_d, the variance of the estimator of the signal. Thus CNR $= N_S/(N_S/\eta_d)^{1/2} = (\eta_d N_S)^{1/2}$, as expected.

For heterodyne detection, the result of measuring the return from a single pulse is a complex number, $r\exp(i\phi)$, equal to D' plus noise, from which an estimate of D' must be derived. As shown in Fig. 1, $r\exp(i\phi)$ is distributed according to Eq. (A1) with $s = N_S^{1/2}$ (without loss of generality, we have set $\phi_S = 0$) and $\sigma = \sigma'$ from Eq. (5). The magnitude, r, is the square root of the number of photons inferred from the measurement: $r = n^{1/2}$. Now $\langle n \rangle = \langle r^2 \rangle = \langle x^2 \rangle + \langle y^2 \rangle$, and the Gaussian moments of Eq. (A1) are easily evaluated to show that $\langle n \rangle = s^2 + 2\sigma'^2$. It is only slightly less easy to use $\langle n^2 \rangle = \langle r^4 \rangle = \langle (x^2 + y^2)^2 \rangle$ to show that $\langle n^2 \rangle = s^4 + 8s^2\sigma'^2 + 8\sigma'^4$ and therefore that the variance of the 1-D distribution of n is

$$\mathrm{Var}(n) = \langle n^2 \rangle - \langle n \rangle^2 = 4s^2\sigma'^2 + 4\sigma'^4$$
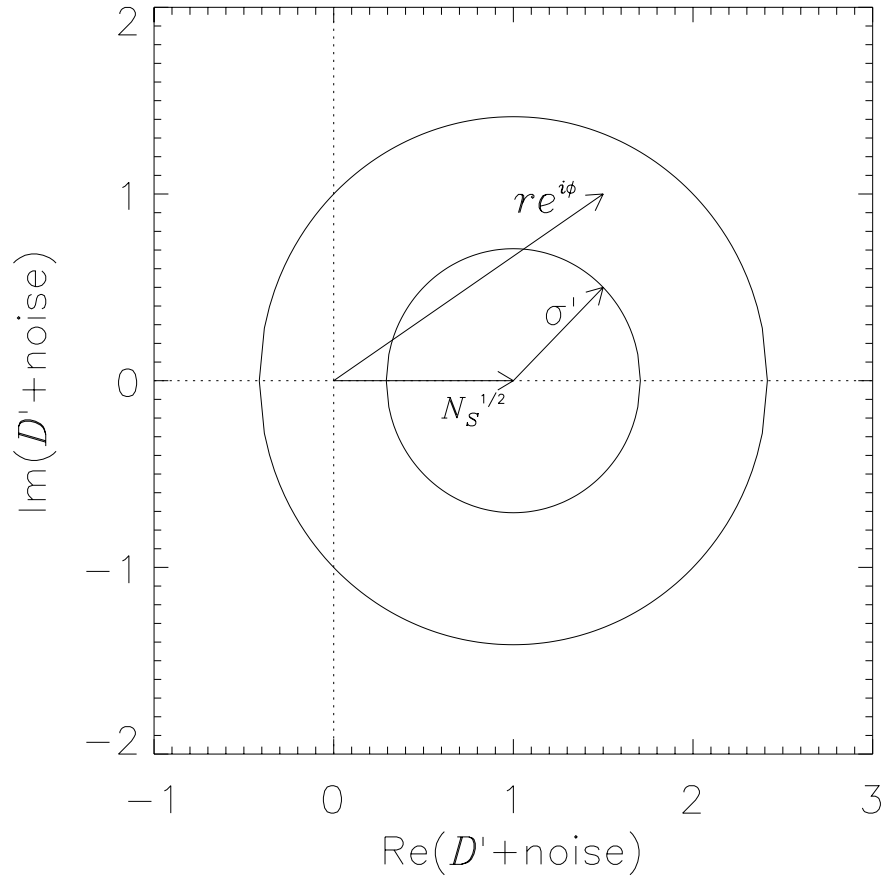$$= 4N_S\sigma'^2 + 4\sigma'^4 \quad . \tag{6}$$

Fig. 1— Distribution of measured values with $N_S^{1/2} = 1$, $\phi_S = 0$, for the ideal case $\sigma'^2 = \frac{1}{2}$ (*i.e.*, $\eta_d = \eta_h = 1$), showing 1- and 2-sigma contours. For the non-ideal case, σ'^2 is increased in accordance with Eq. (5). $re^{i\phi}$ represents a particular measurement taken from this distribution. $r = n^{1/2}$, where n is the number of signal photons inferred from the measurement (see text).

An unbiased estimator of N_S is $n - 2\sigma'^2$, since $\langle n - 2\sigma'^2 \rangle = s^2 = N_S$. Since, from Eq. (5), $\sigma'^2 = $ constant, the variance of this estimator is the same as the variance of n. Using the definition given above, the CNR of heterodyne detection for imaging applications is the ratio of N_S to the standard deviation of its estimator:

$$\mathrm{CNR_{IM}} = \frac{N_S}{\sqrt{\dfrac{2N_S}{\eta_d \eta_h} + \dfrac{1}{\eta_d^2 \eta_h^2}}} \quad \approx \sqrt{\frac{\eta_d \eta_h N_S}{2}} \ \text{ for } N_S \gg 1/(\eta_d \eta_h)$$

$$\approx \eta_d \eta_h N_S \quad \text{ for } N_S \ll 1/(\eta_d \eta_h) \ , \tag{7}$$

where Eqs. (5) and (6) have been used. Taking $\eta_d = \eta_h = 1$ in the first approximation shows that the best possible CNR of heterodyne detection is a factor of $\sqrt{2}$ below the best possible CNR of direct detection. For $N_S \ll 1/(\eta_d \eta_h)$, $\mathrm{CNR_{IM}}$ is proportional to the number of photons detected, rather than to the square

root of this number, a fact that will be revisited in Section 2.4 [see discussion below Eqs. (13) and (14)] where it is found to apply also to the SNR of SA imaging.

Heterodyne detection was first done in RF work, where CNR is defined as the ratio of signal power to noise power, where signal power means the square of the value of the heterodyne-detected signal, which is $(N_S^{1/2})^2 = N_S$, and noise power means $2\sigma'^2$. Thus

$$\mathrm{CNR}_{\mathrm{RF}} = \frac{N_S}{2\sigma'^2} = \eta_d \eta_h N_S = 2\left(\mathrm{CNR}_{\mathrm{IM1}}\right)^2 \; , \qquad (8)$$

where $\mathrm{CNR}_{\mathrm{IM1}}$ is taken from the first approximation in Eq. (7). The first equality in Eq. (8) matches, for two examples, Eq. (12) of Park and Shapiro [8] and Eq. (1) of Shapiro [13], once the conversion to photons has been made. If the RF expression for CNR is used to discuss an optical imaging system, large overstatements of CNR can result, compared to what is normally expected in optical imaging.

In the ideal case, $\eta_d = \eta_h = 1$ and the variance is $2\sigma_o'^2 = 1$. The magnitude of D' is the square root of a (not necessarily integral) number of photons. The units of σ'^2 may therefore be regarded as photons, so that $2\sigma_o'^2 = 1$ photon. This is the variance (in Fourier space) for a measurement done over time interval τ_{pul} and frequency interval $\delta f = 1/\tau_{pul}$, so $2\sigma_o'^2$ may be generalized to $2\sigma_o'^2 = [1 \text{ photon}/(\text{sHz})] \times \tau_{pul}\delta f$, since the time-bandwidth product of the measurement is $\tau_{pul}\delta f = 1$. This generalization illustrates the oft-heard statement that heterodyne detection adds noise at the rate of 1 photon/(sHz). But this statement can be misleading to those accustomed to photon-limited imaging because $2\sigma_o'^2$ is a variance (= noise power), not a standard deviation, and it is the variance of the 2-D distribution of D' plus noise, shown in Fig. 1, not the variance of the 1-D distribution of the number of photons, which is $\mathrm{Var}(n)$, given in Eq. (6). Another way to express this variance is to multiply it by $h\nu$ and write it in terms of power as $2\sigma_o'^2 = h\nu$ W/Hz, or, more generally, as $2\sigma'^2 = h\nu/(\eta_d\eta_h)$ W/Hz. This form, multiplied by a receiver bandwidth, appears as the denominator of the expressions for CNR given by Park and Shapiro [8] and Shapiro [13].

The 1-D distribution of the number of photons can be found from Goodman's [14] Eq. (2.9-20) or (2.9-27). These equations give, respectively, exact and approximate forms of the PDF of $n^{1/2}$ as, in Goodman's notation, $P_A(a)$, where $a = n^{1/2}$. Using $n = a^2$, the PDF transformation method in Goodman's Section 2.5.2 shows that the distribution of the number of photons inferred from a heterodyne detection of N_S is $P_{N_S}(n) = P_A(a)/(2a)$. This distribution is stated as Eq. (19) of Shapiro and Wagner [15], but is not given here because all we need (see Section 2.4) are its first and second moments, $\langle n \rangle$ and $\langle n^2 \rangle$, which have been given above Eq. (6). Since we have not found them in any reference, we exhibit, for small N_S, the uncertainties, Δn and $\Delta\phi$, due to heterodyne measurement of the values of n and ϕ, from which N_S and ϕ_S are estimated. The term uncertainty is used in place of standard deviation because that is the usual terminology of quantum mechanics. We already know from Eq. (6) or the denominator of the first equality in Eq. (7) that $\eta_d\eta_h\Delta n = (2\eta_d\eta_h N_S + 1)^{1/2}$. This way of expressing Δn is chosen because it allows a single curve to show Δn for all values of $\eta_d\eta_h$. We again set $\phi_S = 0$ so $\Delta\phi = \langle\phi^2\rangle^{1/2}$, which can be evaluated by numerical integration using the PDF in Eq. (A1) and $\phi = \tan^{-1}(y/x)$, or using Goodman's Eq. (2.9-25). The result is plotted in Fig. 2, along with $\Delta\sin\phi$ and the products $\Delta n\Delta\phi$ and $\Delta n\Delta\sin\phi$. $\Delta\sin\phi$ is included because $\sin\phi$ rather than ϕ is the true quantum mechanical observable [16]. For $\eta_d = \eta_h = 1$, $\Delta n\Delta\phi \geq 1$ for heterodyne detection, as also found by, for example, Shapiro and Wagner [15].
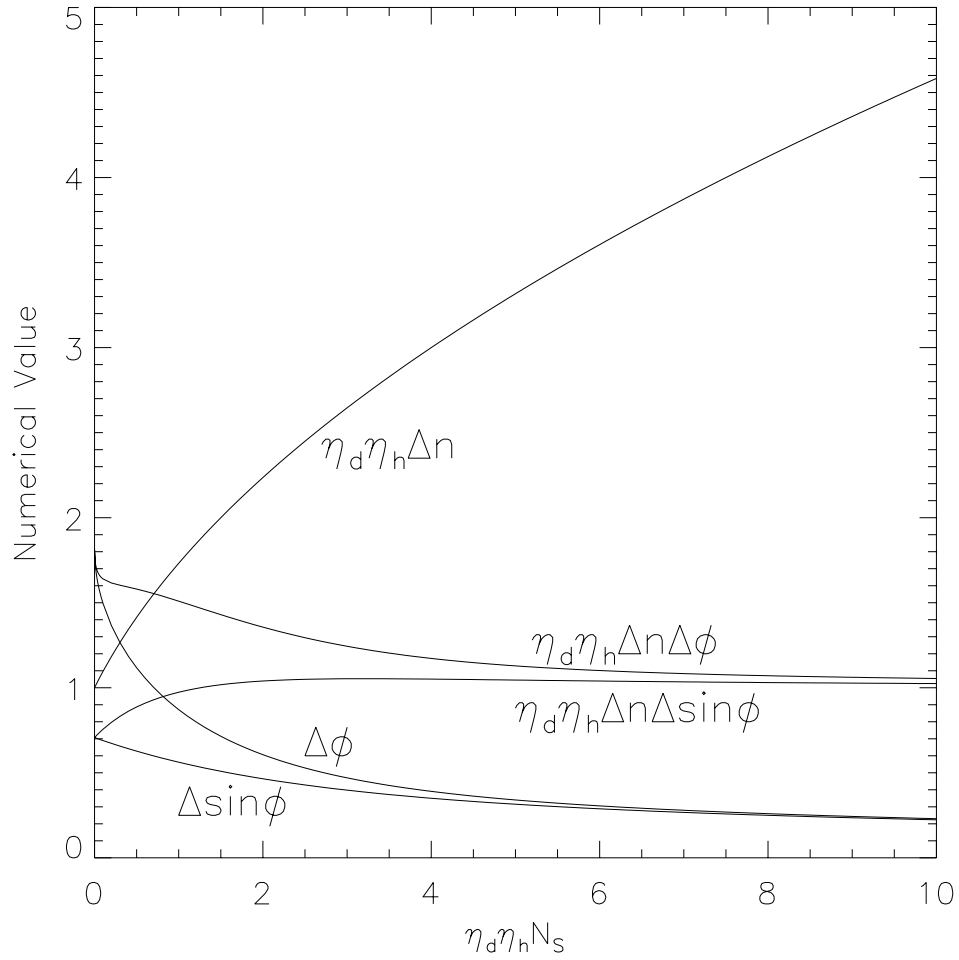
Fig. 2 — Number and phase uncertainties for phase-sensitive heterodyne detection. $\eta_d\eta_h\Delta n = \sqrt{2\eta_d\eta_h N_S + 1}$. For $N_S = 0$, $\Delta\phi = \pi/\sqrt{3}$ and $\Delta\sin\phi = 1/\sqrt{2}$.

2.3 Synthetic Aperture Processing and Phase Errors

Section 2.1 described the measurement of D' plus noise, where D' is the complex amplitude of the wave reflected from one range resolution element and σ' describes the noise of the measurement. Figure 3 shows a range resolution element, divided into M pixels. The pixel labeled $m = 0$ has just entered the illuminated region. Each illuminated pixel contributes a phasor, $A_m = a_m\exp(i\alpha_m)$, with amplitude a_m and intrinsic phase α_m, to D'. The intrinsic phase depends on the detailed structure of the element and on the viewing geometry and may be regarded as random. Thus the average number of photons contributing to D' is the result of the sum of the random phasors A_m, and the discussion in the first paragraph of Appendix A shows that $a_{m,\mathrm{rms}} = (N_S/M)^{1/2}$ in order that the A_m add up to a complex number with magnitude $N_S^{1/2}$.

The phase of each of the A_m is modified by the curvature of the wave front as indicated in Fig. 3. Referenced to zero at the center of the wave front ($m = M/2$), the light described by phasor A_m must travel a greater distance by the amount $\Delta l_m = [(m - M/2)p]^2/R$, where p is the size of a pixel and R is the range, to

return to the detector. A_m is therefore multiplied by the phase coefficient $C_m = \exp(i\Delta l_m \times 2\pi/\lambda)$, and the sum of all these contributions makes up the signal: $D' = \Sigma A_m C_m$. Figure 3 and the expression used for Δl_m assume that the beam direction is exactly perpendicular to the velocity vector of the transmitter. Relaxing this assumption changes the expression for the Δl_m, but not the results of the analysis. The noise, or error, denoted by E_m, adds to the signal to produce the result of a single measurement, $\Sigma A_m C_m + E_m$, as indicated by the first row of Table 1 (less the last column, which indicates multiplication by $C_m{}^*$). The second row shows the contributions to the measurement of the second pulse, when the illuminated region has moved by one pixel, and so on, until the $M - 1$ row describes the pulse having the last contribution from the $m = 0$ pixel. Synthetic aperture processing applies a matched filter to pick out the phase history of a particular pixel as it passes through the beam's footprint. As indicated in Table 1, the filter picks out A_0. Appendix B describes this process in more detail and shows how the high-resolution characteristic of SA processing is obtained. The $C_m{}^*$ are indexed upward by one row to pick out A_1, downward to pick out A_{-1}, etc.

Fig. 3 — Side view of transmitted wave front encountering one range resolution element. Azimuthal resolution elements (pixels) are labeled 0 to *M*-1 (see text). The transmitter is traveling to the left.

Table 1 — Representation of Measurement Composition and Matched-Filter SA Processing

{			A_0C_0	$+ A_1C_1 + \ldots$	$+ A_{M-2}C_{M-2}$	$+ A_{M-1}C_{M-1}$	$+ E_0$ }	$\times C_0^*$
{		$A_{-1}C_0$	$+ A_0C_1$	$+ A_1C_2 + \ldots$	$+ A_{M-2}C_{M-1}$		$+ E_1$ }	$\times C_1^*$
{	$A_{-2}C_0 +$	$A_{-1}C_1$	$+ A_0C_2$	.	.		$+ E_2$ }	$\times C_2^*$
	.	.	.	.	.		.	.
	.	.	.	.	.		.	.
	.	.	.	.			.	.
{$\ldots$ $A_{-2}C_{M-3} +$		$A_{-1}C_{M-2}$	$+ A_0C_{M-1}$				$+ E_{M-1}$}	$\times C_{M-1}^*$
{$\ldots$	≈ 0	≈ 0	MA_0	≈ 0 $\ldots$	≈ 0	≈ 0	$+ G$ }	

For clarity of presentation in Table 1, the profile of the illuminating beam is treated as uniform, when in reality it would have a Gaussian or perhaps an Airy shape. A more careful treatment includes the beam's nonuniform profile in the matched filter, but does not change the final results here or in Appendix B.

The next-to-last column in Table 1 contains the E_m, which are the error contributions from shot noise. The E_m are random numbers distributed according to Eq. (A1) with $s = 0$ and $\sigma = \sigma'$ from Eq. (5). The last column shows the coefficients of the phase history matched filter. These coefficients are calculated from the known geometry of the observation. The bottom row, which is the sum of the rows above it after the multiplications by $C_m{}^*$ have been done, shows the contributions to the output of this filter. The output of the filter is comprised (mostly) of the phasor MA_0 plus noise given by $G = \Sigma E_m C_m{}^*$. The result of

multiplying the random complex number E_m by the unit-magnitude phasor C_m^* is again a random complex number, so G, the sum of M such numbers, is a Gaussian-distributed random complex number with $\sigma''^2 = M\sigma'^2$. The total number of photons from the $m = 0$ pixel in the final image is denoted N_p, so N_p/M are contributed by each pulse, that is, $a_0^2 = N_p/M$. Note that a_0^2 may be small compared to unity. The PDF of $MA_0 + G$ is centered on $Ma_0 = (MN_p)^{1/2}$, while the desired signal is N_p. Therefore, the output of the matched filter must be divided by $M^{1/2}$ to obtain a PDF centered on $N_p^{1/2}$. Accordingly, σ''^2 must be divided by M, returning us to σ'^2 as before. Thus, the error in the output of the matched filter is the same as the error in the measurement of $N_S^{1/2}$, so the PDF for N_p is the same as that given for N_S at the end of Section 2.2, with N_S replaced by N_p. That is, it is $P_{N_p}(n)$, and Var(n) and the CNR for N_p are given by Eqs. (6) and (7) with N_S replaced by N_p.

The average number (averaged over speckle, which is treated in the next section) of photons received per pulse is $N_{S,\text{ave}}$ and the average number of photons per pixel in the final image is $N_{p,\text{ave}}$. Since the photons received from M pulses are distributed over M pixels, $N_{S,\text{ave}} = N_{p,\text{ave}}$, that is, the average number of photons inferred from a single heterodyne detection is the same as the average number in each pixel in the final image.

It was stated above that the C_m^* are calculated from the geometry of the observation. This calculation is a harder problem for SAL than for SAR because the accuracy of the calculation is set by the wavelength of the radiation, which is typically about four orders of magnitude smaller for SAL. (Fortunately, the range need not be known to wavelength accuracy: referring to Fig. 3, it is easy to show that the curvature of a wave front at 999 km range is insignificantly different from its curvature at 1,000 km for the small footprints possible with SAL – see Section 2.5.)

As shown by the above discussion, it is basic to SA imaging that the phase of the light returned from the scene be measured. Ideally, the phase of the light emitted by the laser would be constant over the entire imaging time, τ_{im}, but this is not essential: only phase knowledge is required, not phase accuracy. In principle, if phase errors are known, compensating corrections can be applied to the digitized data. This problem has received much attention from SAR workers, especially with regard to the effects of having imperfect knowledge of the platform's motion: if the platform is one-half wavelength closer to the scene than expected upon reception of a pulse, a phase error of 180° is incurred. This means that the matched filter coefficient applied to the digitized data from this pulse will be in error by a factor of exp($i\pi$) and will fail to pick out the right phasor, as described above (cf. especially Table 1). If phase errors this large occur on a pulse-to-pulse basis, then the data are reduced to hash and no image can be recovered. But, as discussed by, for example, Jakowatz et al. [5], if phase errors occur more slowly, a rough image can be generated and serve as the basis for "auto-focusing" algorithms to correct the phase of each pulse in software and render the image sharp. These techniques can be carried over to SAL if the hardware can keep phase error rates to the low level required. In the baseline imaging scenario of Section 2.5, the dwell time is $\tau_{dw} = 1.7$ ms and 100 pulses are sent during this time, one every 17 μs. Ideally, phase errors would be small over 1.7 ms, but auto-focusing requires only that phase errors be small over the time between pulses (17 μs), a factor of 100 ($= M$) relaxation of the requirement.

Another source of phase errors is the passage of the beam through the atmosphere. Now, if the atmosphere simply changed the phase of the wave returned from the scene by a fixed amount, it would be indistinguishable from the scene itself (recall that scattering from a conventional surface — as opposed to, say, a mirror — randomizes phase) and no problem would be encountered. But as the satellite moves, the line of sight from the satellite to a particular pixel on the ground follows a (slightly) different path through the atmosphere. If this different path imposes a significantly different phase change than the previous one,

it will disrupt the phase history of the pixel and inhibit our ability to form a good image. This point is discussed further in Section 2.7.

Unlike SAR, for SAL the stability of the LO cannot be taken for granted, which is another source of phase errors. From a range of 1,000 km, the round-trip time of flight is about 7 ms. In order for the LO to maintain its phase over this time period, it must have a linewidth of about 100 Hz or better. This is a formidable requirement for a laser, especially a power laser. The solution will probably be an extremely stable reference laser against which the phase errors of the power laser can be measured.

2.4 Speckle and SNR

The most severe limit on an imaging system that uses coherent light is speckle. In the foregoing, the variance due to shot noise of a single pixel in the final SA image has been calculated. But if that pixel were viewed from a different direction, the sensor would be in a different part of the pixel's speckle field and a different value of N_p would be observed. Or if there are many pixels in the scene with the same reflection properties, they will produce different values of N_p because different parts of their speckle fields are sampled. To find the resulting SNR in an image, the speckle and shot noise contributions to variance must be combined.

With $s = 0$, Eq. (A1) describes the phasor distribution of speckle. The resulting intensity PDF [see Goodman [14], Eq. (7.5-1)] is,

$$P_S\left(N_p\right) = \frac{1}{N_0}\exp\left(-\frac{N_p}{N_0}\right),\tag{9}$$

where $N_0 = \langle N_p\rangle$ is the average of N_p taken over many realizations of speckle. The second moment of this distribution is $\langle N_p^2\rangle = 2N_0^2$, so the variance is $\mathrm{Var}(N_p) = N_0^2$. This leads to the familiar result that the SNR due to speckle for a single polarization is unity: $\mathrm{SNR} = N_0/[\mathrm{Var}(N_p)]^{1/2} = 1$. Equation (9) is given as a continuous function. In high-intensity speckle, this is justified because $N_0 \gg 1$; in our case, it is justified because both N_p and N_0 are averages and are normally not integers.

For a fixed realization of speckle, the variation in the number of photons, n, that contribute to a particular pixel in a single image is due only to shot noise from the heterodyne detection. The PDF of this 1-D distribution, $P_{N_p}(n)$, was introduced at the end of Section 2.2. As discussed there, we have not calculated $P_{N_p}(n)$ explicitly, but, using $s^2 = N_p$ in the expressions for $\langle n\rangle$ and $\langle n^2\rangle$ given above Eq. (6), have calculated its first moment to be $N_p + 2\sigma'^2$ and its second to be $N_p^2 + 8N_p\sigma'^2 + 8\sigma'^4$. Combining the distribution of speckle realizations given by Eq. (9) with $P_{N_p}(n)$ gives the total probability of getting a particular value n:

$$P_T\left(n\right) = \int_0^\infty P_{N_p}\left(n\right)P_S\left(N_p\right)dN_p,\tag{10}$$

which may be stated in words as the probability of measuring the value n given N_p, summed over the probability of N_p. The moments of n are

$$\langle n \rangle = \int_0^\infty n P_T(n)\, dn = \int_0^\infty \int_0^\infty n P_{N_p}(n)\, dn\, P_S(N_p)\, dN_p$$

$$= \int_0^\infty \left(N_p + 2\sigma'^2 \right) P_S(N_p)\, dN_p \qquad (11)$$

$$= N_0 + 2\sigma'^2 \quad ,$$

as expected, and

$$\left\langle n^2 \right\rangle = \int_0^\infty \int_0^\infty n^2 P_{N_p}(n)\, dn\, P_S(N_p)\, dN_p$$

$$= \int_0^\infty \left(N_p^2 + 8 N_p \sigma'^2 + 8\sigma'^4 \right) P_S(N_p)\, dN_p \qquad (12)$$

$$= 2 N_0^2 + 8 N_0 \sigma'^2 + 8\sigma'^4 = 2(N_0 + 2\sigma'^2)^2 \quad ,$$

so $\mathrm{Var}(n) = (N_0 + 2\sigma'^2)^2$, and, using σ'^2 from Eq. (5), the SNR for photon-limited SA imaging is

$$\mathrm{SNR}_{\mathrm{SA}} = \frac{N_0}{N_0 + 1/(\eta_d \eta_h)} \quad \begin{array}{ll} \approx 1 & \text{for } N_0 \gg 1/(\eta_d \eta_h) , \\[2mm] \approx \eta_d \eta_h N_0 & \text{for } N_0 \ll 1/(\eta_d \eta_h) , \\[2mm] = 1/2 & \text{for } N_0 = 1/(\eta_d \eta_h) . \end{array} \qquad (13)$$

These steps can be repeated for direct detection: in Eqs. (11) and (12), $P_{N_p}(n)$ is replaced by the Poisson distribution having mean $\eta_d N_p$ and the integral over n by the discrete sum over n appropriate for a Poisson distribution. The results are $\langle n/\eta_d \rangle = N_0$, $\langle (n/\eta_d)^2 \rangle = 2 N_0^2 + N_0/\eta_d$, and $\mathrm{Var}(n/\eta_d) = N_0^2 + N_0/\eta_d$, so the SNR for photon-limited direct detection (DD) of one polarization of coherent light is

$$\mathrm{SNR}_{\mathrm{DD}} = \sqrt{\frac{N_0}{N_0 + 1/\eta_d}} \quad \begin{array}{ll} \approx 1 & \text{for } N_0 \gg 1/\eta_d , \\[2mm] \approx \sqrt{\eta_d N_0} & \text{for } N_0 \ll 1/\eta_d , \\[2mm] = \sqrt{\dfrac{N_0}{N_0 + 1}} & \text{for } \eta_d = 1 , \end{array} \qquad (14)$$

which, for $\eta_d = 1$, is the same as Goodman's [14] Eq. (9.2-18) once the identification $\overline{K} = N_0$ has been made.

We now relate $\mathrm{SNR}_{\mathrm{SA}}$ to $\mathrm{SNR}_{\mathrm{RF}}$, the expression for SNR used by the RF community. The relation between $\mathrm{SNR}_{\mathrm{RF}}$ and $\mathrm{CNR}_{\mathrm{RF}}$ in the presence of speckle can be found from Eq. (4.10) of Shapiro et al. [7], which shows the relation for an arbitrary random process. The intention of Shapiro et al. is that the random process is turbulence, but the formula can also be used for speckle. Putting the statistical property of speckle that the variance equals the square of the mean [this was written above as $\mathrm{Var}(N_p) = N_0^2$, in Shapiro et al.'s notation it is $\mathrm{Var}(|\mathbf{y}|^2) = \langle |\mathbf{y}|^2 \rangle^2$] into Eq. (4.10), and using Eq. (4.11) and our Eq. (8) with $N_S = N_0$ shows that

$$\mathrm{SNR}_{\mathrm{RF}} = \frac{\mathrm{CNR}_{\mathrm{RF}}/2}{1+\mathrm{CNR}_{\mathrm{RF}}/2+(2\mathrm{CNR}_{\mathrm{RF}})^{-1}}$$

$$= \left[\frac{\mathrm{CNR}_{\mathrm{RF}}}{\mathrm{CNR}_{\mathrm{RF}}+1}\right]^2 = \left[\frac{N_0}{N_0+1/(\eta_d\eta_h)}\right]^2 = (\mathrm{SNR}_{\mathrm{SA}})^2 \ . \tag{13a}$$

Observe that when $\mathrm{SNR}_{\mathrm{SA}} = \frac{1}{2}$, $\mathrm{SNR}_{\mathrm{RF}} = \frac{1}{4} = -6$ dB.

Equations (13) and (14) show the saturation effect [7] expected when speckle is the dominant source of noise: when $N_0 >> 1/(\eta_d\eta_h)$, SNR ≈ 1 in both cases and higher values of N_0 do not improve SNR. When $N_0 = 1/(\eta_d\eta_h)$, the SNR of SAL imagery is $\frac{1}{2}$ – only a factor of two below the limiting value of 1. SNR can, of course, be improved at the cost of complexity by measuring both polarizations, at the cost of resolution by combining pixels in one image, as is often done for SAR, and/or at the cost of more observation time by combining images that sample different parts of the speckle field.

For small N_0, $\mathrm{SNR}_{\mathrm{SA}}$ is proportional to the number of photons detected, while $\mathrm{SNR}_{\mathrm{DD}}$ has the more familiar property of being proportional to the square root of this number. Now, if multiple images from uncorrelated parts of the speckle field are added together, both $\mathrm{SNR}_{\mathrm{SA}}$ and $\mathrm{SNR}_{\mathrm{DD}}$ improve only as the square root of the number of images combined (this is the normal statistical expectation, see also p. 217 of Curlander and McDonough [4]). This means that it is much harder to make up for a low count rate by adding SA images, compared to DD images, as the following numerical example shows. Taking $\eta_d = \eta_h = 1$ for simplicity, $N_0 = 0.1$ implies $\mathrm{SNR}_{\mathrm{SA}} \approx 0.1$ and $\mathrm{SNR}_{\mathrm{DD}} \approx 0.3$. It takes nine images to improve $\mathrm{SNR}_{\mathrm{DD}}$ to 0.9, but 81 to improve $\mathrm{SNR}_{\mathrm{SA}}$ to 0.9. This shows the importance of designing an SA system to meet the criterion $N_0 = 1/(\eta_d\eta_h)$ for single-look imagery implied by Eq. (13). If this condition is not met, very many single-look images will have to be combined just to approach an SNR of unity.

The astute reader may ask about taking the multiple images while maintaining phase coherence across a larger part of the speckle field, i.e., using a larger SA. But with, say, twice the SA, SA processing yields twice as many pixels, each having half the extent in the azimuth direction as the original and each receiving the same number of photons as the original pixel. Adding these pixels together to match the original pixel improves $\mathrm{SNR}_{\mathrm{SA}}$ by $\sqrt{2}$, the same result as adding two successive, separately processed images, so the improvement is the same whether the multiple images are taken coherently or incoherently.

2.5 Space-Based SAL Design Equations

In Section 2.4, we showed that the total number of photons present at the detector from one pixel in the scene needs to be $N_0 \approx 1/(\eta_d\eta_h)$ for a worthwhile SNR in an image (multiple images can then be added to improve SNR in the usual way). In this section, we calculate the number of photons per pixel that would be received by an orbiting SAL. Parameters are given below for a baseline system using 2 μm light and for a variation using 10 μm light. The baseline system assumes a beam footprint of 10 m and a resolution of 0.1 m. The 10-m footprint exposes a basic limitation of SAL – supplying enough photons to cover a substantially larger footprint requires prohibitive laser power. A range of 1,000 km is chosen to give an easily scaled parameter that is approximately a geometric mean between the minimum and maximum distances (100 – 10,000 km) at which use is contemplated. The footprint size is assumed to be determined by the diffraction limit of the transmitting aperture. Circular apertures for the transmit and receive optics are assumed, but the area ratio of circles to squares ($\pi/4$) is ignored. Also ignored is the difference between the resolution measured perpendicular to the beam and measured on the ground. With the resolution measured perpendicular to the beam, the pixels are assumed square, that is, when the ground

surface is inclined at 45° with respect to the beam, the laser is assumed to have sufficient chirp capability to yield the same cross-track resolution as SA processing yields in the azimuth (along-track) direction. An orbital speed of 6 km/s is used because it is reasonably accurate for low and medium orbital altitudes. Even for extremely elliptical orbits, the speed of the satellite differs from 6 km/s by less than a factor of two as long as the orbit's apogee is no more than about 10,000 to 12,000 km.

A degree of flexibility that is essential to an effective SAL is added by assuming that the beam can be rapidly repositioned, either by steering the beam or rotating the satellite, so that a footprint can be scanned more than once and/or neighboring footprints can be covered. This capability is needed to make up for the low SNR and small footprint inherent to SAL. Beam repositioning allows improvements in SNR by taking images from different parts of the speckle field and in area coverage by taking a mosaic of images. Further, we assume that coherence can be maintained for up to N_{sc} scans of the same footprint, so that multiscanning can also improve resolution. $N_{sc} = 1$ for normal scan mode operation, and in this mode SA processing is contained in the assumption that the pixel size p is one-half the diameter of the transmitting aperture D_T as shown in Eq. (B5). Scanning the footprint N_{sc} times means that the platform traverses an N_{sc}-times-longer synthetic aperture and, therefore, that the resolution of the image can be N_{sc} times better, i.e., that the pixel size is given by $p = D_T/(2N_{sc})$. If N_{sc} is allowed to become large, this process approaches spotlight-mode SA imaging [5], a subject that is not explicitly considered here, but for which the formulas given below remain valid. The total dwell time τ_{dw} is defined to be the time that a single point on the ground is illuminated by the beam. This is the time it takes to move the beam the length of the footprint at the speed of the orbiting platform, multiplied by N_{sc} to account for multiple scans. In order for all points in a single ground footprint to have complete phase histories, i.e., to be moved completely through the beam, the beam must move two ground footprints in each scan. Thus, the time it takes to generate a complete image of one footprint is $2\tau_{dw}$, referred to as the imaging time τ_{im}.

SAR systems normally use the same antenna for transmission and reception, but this is not essential for SA imaging. For SAL, the receiver will be assumed to have a different aperture, with K-times-larger diameter than the transmitter. The K-times-larger aperture collects K^2 as much light from a ground pixel and has a K-times-smaller footprint than the transmitter. There must therefore be K^2 heterodyne detectors in the focal plane of the receiver instead of one, and light from the first M/K pixels shown in Fig. 3 is detected by one of these, light from the next M/K pixels by another, and so on. Thus, the phase history of a pixel indicated in Table 1 must be traced through the outputs of K detectors. There is no problem with this in principle, "only" in engineering.

Basic design parameters (general terms and a numerical example are given)

1) $\lambda = 2\ \mu m = 2 \times 10^{-6}$ m
2) P = laser output power = 1 kW (time-averaged)
3) transmit optics area = $D_T^2 = (0.2\ m)^2$
4) receive optics area = $D_R^2 = K^2 D_T^2 = (1\ m)^2\ (\Rightarrow K^2 = 25)$
5) R = range to scene = 1,000 km = 10^6 m
6) V = platform speed $\approx 6 \times 10^3$ m/s (orbital altitude $\le$ 10,000 km)
7) ρ = surface reflectance = 0.1 (changes with wavelength), Lambertian distribution
8) η_t = combined transmission efficiency of transmit and receive optics and atmosphere = 0.5
9) N_{sc} = number of scans of footprint = 1

Derived quantities

1) F = footprint size = $(\lambda/D_T)R = 10$ m $(\Rightarrow D_T = \lambda R/F)$
2) p = pixel size = $D_T/(2N_{sc}) = 0.1$ m (from SA processing)

3) Ω = collection solid angle = $D_R^2/R^2 = [(1\ \text{m})/(10^6\ \text{m})]^2 = 10^{-12}$ ster
4) τ_{dw} = dwell time = ($N_{sc} \times$ footprint length)/(platform speed) = $N_{sc}F/V$ = 1.7 ms
5) $\tau_{im} = 2\tau_{dw}$ = imaging time = 3.3 ms
6) M = number of pulses that illuminate one pixel = F/p = 100
7) τ_{pul} = pulse time $\leq \tau_{dw}/M = N_{sc}p/V$ = 17 μs

Derived quantities 6 and 7 are determined by the SA processing requirement that there be one transmitted pulse per azimuthal resolution element. The pulse repetition frequency (PRF) is

$$\text{PRF} = \frac{V}{N_{sc}\,p} = 6 \times 10^4 \left(\frac{1}{N_{sc}} \right) \left(\frac{0.1\,\text{m}}{p} \right) \left(\frac{V}{6\,\text{km/s}} \right) \ \text{pulses/s.} \tag{15}$$

We saw in Eq. (4) that the Nyquist criterion requires that each pulse be sampled at least $2M$ times to recover M range resolution elements, so the data sampling rate SR must be SR $\geq 2M/\tau_{pul} \geq 2FV/(N_{sc}p^2)$ = 12 MHz for the numerical example, a modest requirement.

To see what the frequency range of the laser's chirp must be, we first observe that the two-way transit time of a wave front across a range increment δl is $\delta t = 2\delta l/c$. In Eq. (3), we saw that if the laser's frequency is varied linearly through a total chirp range Δf_{ch} in the time τ_{pul} ($\dot f = \Delta f_{ch}/\tau_{pul}$), the change in beat frequency caused by the time increment δt is $\delta f = 2(\Delta f_{ch}/\tau_{pul})(\delta l/c)$. We have already seen that the minimum detectable frequency difference is $\delta f = 1/\tau_{pul}$, so, setting $\delta l = p$ (if the surface is inclined at 45°, a range resolution of p implies an image resolution of p measured perpendicular to the beam and $\sqrt 2\ \text{p}$ measured along the surface), we find

$$\Delta f_{ch} = \frac{c}{2p} = 1.5 \left(\frac{0.1\,\text{m}}{p} \right) \text{GHz.} \tag{16}$$

The length of the synthetic aperture is the distance traversed by the platform in the dwell time. It can be written in a number of useful forms, some of which are

$$L_{SA} = V\tau_{dw} = N_{sc}F = \frac{\lambda R}{2p}. \tag{17}$$

The diameter of the transmitter needed to give the desired footprint and the consequent pixel size that results from SA processing are related by

$$D_T = 2N_{sc}\,p = \frac{\lambda R}{F} = 0.2 \left(\frac{\lambda}{2\,\mu} \right) \left(\frac{10\ \text{m}}{F} \right) \left(\frac{R}{1{,}000\,\text{km}} \right)\ \text{m.} \tag{18}$$

The time-averaged laser power within the usable footprint is taken to be $P/2$. The power per unit solid angle scattered from the surface, assumed Lambertian, is then

$$J = \frac{P}{2}\frac{\rho\cos\theta}{\pi}\ \ \text{W/ster,} \tag{19}$$

where θ is an observation angle. We take $\cos\theta \approx 1$, and multiply by the transmission efficiency to find that the power collected from the footprint and impinging on the detector is

$$P_F = \frac{P}{2}\frac{\rho}{\pi}\Omega\eta_t = \frac{P}{2\pi}\frac{D_R^2}{R^2}\rho\eta_t \text{ W}. \tag{20}$$

The conversion factor to photons is $5 \times 10^{24} \times \lambda$ photons/j when λ is expressed in meters, so the photon rate is $5 \times 10^{24} \times \lambda P_F$. The total number of photons per pixel impinging on the detector in one polarization is this rate multiplied by the dwell time, by the fractional area of the footprint covered by one pixel, and by ½ to account for polarization. Using the synthetic aperture condition $N_{sc} = \lambda R/(2pF)$ from Eq. (18) and $\tau_{dw} = N_{sc}F/V = \lambda R/(2pV)$, this is

$$N_0 = \frac{1}{2}\times 5\times10^{24}\lambda P_F\tau_{dw}\left(\frac{p}{F}\right)^2 = 5\times10^{24}\lambda\frac{P}{4\pi}\frac{D_R^2}{R^2}\rho\eta_t\frac{\lambda R}{2pV}\left(\frac{p}{F}\right)^2 = 5\times10^{24}\frac{P}{8\pi}\frac{\lambda^2}{F^2}\frac{pD_R^2}{RV}\rho\eta_t$$

$$= 6.6\left(\frac{P}{1\,\text{kW}}\right)\left(\frac{\lambda}{2\,\mu}\right)^2\left(\frac{10\,\text{m}}{F}\right)^2\left(\frac{p}{0.1\,\text{m}}\right)\left(\frac{D_R}{1\,\text{m}}\right)^2\left(\frac{1,000\,\text{km}}{R}\right)\left(\frac{6\,\text{km/s}}{V}\right)\left(\frac{\rho}{0.1}\right)\left(\frac{\eta_t}{0.5}\right)\text{ photons.} \tag{21}$$

Equations (18) and (21), along with the criterion from Eq. (13) that $N_0 = 1/(\eta_d\eta_h)$ provides a near-saturation SNR, contain most of the high-level information needed to decide if a notional design is adequate. The laser required to implement the design must have the capabilities given in Eqs. (15) and (16). We expect to find $1/(\eta_d\eta_h) \approx 2 - 4$ in a well-designed system, so Eq. (21) indicates that the illustrative system is viable. Putting typical SAR parameters into Eq. (21), $P \approx 200$ W, $\lambda \approx 2$ cm, $F \sim 20$ km, $p \sim 2$ m, $D_R \sim 5$ m, gives $N_0 \sim 10^5$ photons, which shows why SAR workers don't worry about photon statistics. Equations (18) and (21) are design equations used to determine the hardware parameters (λ, P, D_T, D_R, N_{sc}) needed to produce the desired end-use parameters (p, F, R). We can substitute $\lambda R/F = D_T$ from Eq. (18) into Eq. (21) to find that

$$N_0 = 5\times10^{24}\frac{P}{8\pi}\frac{pD_T^2 D_R^2}{R^3V}\rho\eta_t, \tag{22}$$

which shows how the signal scales with range, keeping constant resolution, once the hardware parameters are fixed. Observe that Eq. (22) is independent of λ.

Equation (21) shows the advantage of using the longest wavelength that can give the desired information and/or is technically feasible on a spacecraft: the longest wavelength tends, depending on choices of the other parameters, to produce the largest N_0. The ability to use $N_{sc} > 1$ provides a means of achieving the same footprint and resolution with a longer wavelength by increasing λ and N_{sc} (and D_T) proportionately in Eq. (18). This allows N_0 to be increased and/or laser power to be reduced in Eq. (21), and reduces the PRF given in Eq. (15). An alternative to the baseline design that requires much less laser power and reasonable mirror sizes is $\lambda = 10$ μ, $D_T = D_R = 1$ m (common transmit and receive aperture, which provides the simplification that $K = 1$), and $N_{sc} = 5$. This does incur the relatively mild penalty that the reflectivity of most surface materials tends to be low ($\sim 5\%$) in this spectral region, but allows $N_0 = 5$ with $P = 80$ wt. If D_R can be larger than one meter, laser power can be further reduced.

The imaging time can be expressed in similar parametric form as

$$
\tau_{im} = \frac{2N_{sc}F}{V} = \frac{\lambda R}{pV}
$$

$$
= 3.3 \times 10^{-3} \left(\frac{\lambda}{2\mu} \right) \left(\frac{0.1\,\mathrm{m}}{p} \right) \left(\frac{R}{1,000\,\mathrm{km}} \right) \left(\frac{6\,\mathrm{km/s}}{V} \right) \mathrm{s} ,
$$

(23)

so the area coverage rate is

$$
\frac{\mathrm{area}}{\mathrm{time}} = \frac{F^2}{\tau_{im}} = \frac{pVF^2}{\lambda R}
$$

$$
= 3 \times 10^4 \left(\frac{2\mu}{\lambda} \right) \left(\frac{p}{0.1\,\mathrm{m}} \right) \left(\frac{F}{10\,\mathrm{m}} \right)^2 \left(\frac{1,000\,\mathrm{km}}{R} \right) \left(\frac{V}{6\,\mathrm{km/s}} \right) \mathrm{m}^2/\mathrm{s} .
$$

(24)

Kyle [9] evaluates a SAL system for the Earth in much the same way as presented in Eq. (21), but does not reduce the result to photons. In our notation, he uses $P = 10$ wt, $\lambda = 10\,\mu$, $p = 0.1$ m, $D_T = D_R = 0.2$ m, $R = 200$ km, $\rho = 1$, $\eta_t = 1$, and $V = 8 \times 10^3$ m/s. Comparing his Eqs. (3) and (4a) shows that his footprint size, denoted D' by him in his Eqs. (2) and (3) and D_I in his Eqs. (10) – (15), is $D' = D_I = F = 10$ m. Putting these values into Eq. (21) and multiplying by two to include both polarizations yields $N_0 = 9$ photons, which makes the system viable by our definition (aside from the unrealistic assumptions about reflectivity and transmission efficiency, and no consideration given to degradation of beam quality due to propagation through the atmosphere), but falls about two orders of magnitude short of supporting the claim made in the fourth paragraph of his Section V that the $\mathrm{CNR_{RF}}$ is 331 (Kyle does not consider speckle, so $N_0 = N_p$ and his SNR is our $\mathrm{CNR_{RF}}$). Kyle's basic error appears to be failing to recognize the discrepancy between (a) the bandwidth needed to match the pulse width of $\Delta t = 0.23$ ns stated by him as necessary to give the range resolution specified in his Eq. (19), and (b) the bandwidth from his Eq. (5a) on which the noise expression in his Eq. (16) is based. A wider bandwidth in his Eq. (16) would result in a lower SNR in his Eq. (17). Stated as a time, rather than bandwidth, discrepancy, Kyle's dwell time is $\tau_{dw} = D_I/V = 10/8{,}000 = 1.25$ ms, and he states that there are N^2 pulses in this time, which, with $N = 100$ (as implied by a footprint of 10 m and a resolution of 0.1 m), implies a pulse time $\Delta t = 0.125\,\mu$s, nearly three orders of magnitude greater than 0.23 ns. Kyle does not address this discrepancy. If the 0.125 µs value is substituted into Kyle's Eq. (15), we find $D_I = 10$ m, as expected; if 0.23 ns is used we find $D_I = 5{,}430$ m. Neither value matches Kyle's statement in the sixth paragraph of his Section V that $D_I = 543$ m.

2.6 Object Motion Sensitivity

SAL is sensitive to motion in the scene, just as SAR is. Consider Fig. 3, the discussion of phase history in Section 2.3, and Appendix B, especially Eq. (B1). Suppose that pixel zero consists of an object moving toward the sensor at speed v. If, during the time $\tau_{dw} = N_{sc}F/V$ that the footprint takes to cross the object N_{sc} times, it moves a distance $\lambda/2$, then the phase of the light returned from this point of the scene changes by the unexpected increment $-2\pi/M$ for each of the M pulses. This means that when the sum $\Sigma A_0 C_m C_m^*$ is evaluated to find the content of pixel zero, the phasors wrap to zero and the sum is zero instead of MA_0: pixel zero appears to be empty (aside from noise and small contributions from other pixels). But when the C_m^* are indexed upward to pick out A_1, the C_{m+1}^* in the sum $\Sigma A_0 C_m C_{m+1}^*$ compensate for the unexpected

phase change and the result is $(M-1)A_0$: the content of pixel zero is added into pixel 1. Thus, the object speed required to move a pixel by one resolution element in the azimuth direction is

$$v_{az1} = \frac{\lambda/2}{\tau_{dw}} = \frac{\lambda VR}{2N_{sc}FR} = \frac{V}{R}p = 0.6 \ \ \text{mm/s,} \tag{25}$$

where $p = D_T/(2N_{sc}) = \lambda R/(2N_{sc}F)$ has been used, and the numerical value is taken from the parameters in Section 2.5. Equation (25) applies to SAR as well as SAL, the difference between the two being only that SAL is expected to have one to two orders of magnitude better resolution (smaller p) than SAR, hence is more sensitive to object motion by the same factor.

The speed required to move a pixel by one resolution element in the range direction is found by evaluating the Doppler shift. An object moving toward the sensor at speed v imposes a Doppler shift of $\delta f_D = 2v/\lambda$. We have already seen in Section 2.1 that the frequency increment in the heterodyne detection that corresponds to one range resolution element is $\delta f = 1/\tau_{pul}$. We now write $\tau_{pul} = \alpha\tau_{dw}/M$, where α, $0 < \alpha \le 1$, is the duty cycle of the laser (cf. derived quantity 7 in Section 2.5), and set $\delta f = \delta f_D$ to find that

$$v_{r1} = \frac{M\lambda}{2\alpha\tau_{dw}} = \frac{M}{\alpha}v_{az1} = 60 \ \ \text{mm/s,} \tag{26}$$

where $\alpha = 1$ has been assumed for the numerical example. Equation (26) gives the speed needed to cause an object to appear in the adjacent range resolution element. If the object is near the edge of a footprint, then, depending on the direction of the motion, a speed a few times larger than v_{r1} may remove it from the image entirely. Since the footprint is M resolution elements across, a speed of $Mv_{r1} = 6$ m/s will remove the object from the image regardless of its true location. Since 6 m/s is about 13 mph or 11 knots, it appears that SAL will not be useful for observing ships at sea or, because of wave motion, the sea surface itself.

2.7 Isoplanatic Angle of the Atmosphere

The primary atmospheric effect of concern to SAL is distortion of the returning wave front, caused by turbulence. It is well known that if two light rays pass side-by-side through the atmosphere, coherence between them will be nearly unaffected as long as the distance between them does not exceed a small value referred to as the coherence, or isoplanatic, length, typically $0.1 – 1$ m, depending on the state of the atmosphere and the wavelength of the light. To maintain phase coherence for the entire time of image formation, the transmitted pulses must all travel through an isoplanatic region of the atmosphere. This means that, as viewed from the ground observation point, the angular motion of the platform must remain within an isoplanatic angle of the atmosphere during the period in which the pulses are transmitted. If this is not the case, then the phase of the last returned pulse will differ from that of the first by an unknown, atmosphere-dependent amount and the output of the matched filter will not be the desired quantity. At $\lambda = 2 \ \mu$, the isoplanatic angle of the atmosphere is typically $\Delta\theta_{iso} = 20 – 40 \ \mu$rad (at a good site) and scales as $\lambda^{6/5}$. The angular speed of the platform with respect to the ground is V/R, so the time it takes the platform to cross an isoplanatic angle is

$$\tau_{iso} = \frac{\Delta\theta_{iso}}{V/R} = (20 - 40) \times 10^{-6} \left(\frac{\lambda}{2\mu}\right)^{6/5} \frac{R}{V}$$

$$= (3.3 - 6.7) \times 10^{-3} \left(\frac{\lambda}{2\mu}\right)^{6/5} \left(\frac{R}{1,000\,\text{km}}\right) \text{ s.}$$

(27)

Comparing Eqs. (23) and (27) shows that

$$\frac{\tau_{im}}{\tau_{iso}} = (0.5 - 1.0) \times \left(\frac{2\mu}{\lambda}\right)^{1/5} \left(\frac{0.1\,\text{m}}{p}\right) ,$$

(28)

which indicates that our example system is marginally within the limits imposed by the atmosphere, at least under good conditions. Park and Shapiro [7] reached a similar conclusion.

If $\tau_{im} > \tau_{iso}$, phase errors introduced by the atmosphere begin to enter. Now, as discussed in Section 2.3, phase errors introduced by platform jitter may be correctable if they are sufficiently slowly varying, and at first glance the same would appear to be true for atmosphere-induced phase errors. But jitter-induced phase errors are constant across the beam's ground footprint (i.e., are the same for all pixels, which is what makes their correction possible), while atmospheric phase errors are constant only across a coherence length of the atmosphere (typically < 1 m), and can vary considerably across a footprint (typically ≥ 10 m). Removing errors of this type by data processing is much more problematic. If D_R is sufficiently greater than D_T that one resolution element of the receiving optics is about the same size as one coherence length, then correcting atmospheric phase errors in data processing appears feasible, but again adds the complication, as discussed in Section 2.5, that multiple heterodyne receivers must be placed in the focal plane. Further consideration of this problem shows that adaptive optics are of no use to a space-based SAL because the atmosphere is close to the scene, not close to the receiver (the opposite of the case in astronomy). This means that phase errors cannot be corrected in the optics' pupil plane – which is what adaptive optics do. For an air-based SAL, adaptive optics may be of some use, but would be a complicated means of achieving a probably marginal performance improvement.

Observe that Eq. (28) depends almost exclusively on resolution and suggests, depending on the effectiveness of phase error correction techniques, a minimum attainable resolution for Earth observations: if the desired pixel size is too small, then the size of the SA is too big, and the paths of the light rays cannot be confined to a sufficiently small range of angles as they pass through the atmosphere.

3. LABORATORY DEMONSTRATION

3.1 Background

One-dimensional imaging with either FM chirping or reconstructed phase history is fairly straightforward in the optical domain. Detection of 1-D range information with an FM-chirped system can be done relatively easily since tracking of the optical phase is not required. Also, 1-D image information from reconstructed phase history is relatively easy to obtain with a single-frequency laser. Thus, 1-D ladar systems using pulse-echo [17], FM chirping with coherent detection [17,18], and SA processing with reconstructed phase histories [2,9,19] have been reported. Also a range-Doppler ladar system [20] and a stepped-frequency, tilt-mirror system [10] requiring 2-D scanning with a potential to produce 3-D images have been investigated. But full 2-D implementation of a synthetic aperture imaging ladar, a long-sought goal, has not previously been demonstrated.

A number of difficulties prevent a straightforward duplication of SAR 2-D imaging techniques in the optical domain. Because the optical field cannot be detected directly, coherent detection must be used to retrieve the range and optical phase. The phase tracking has to be done on a micron instead of on a centimeter scale, the received signal is very weak, and atmospheric turbulence effects play a role. We report here the first demonstration of a full 2-D SAL system using both phase history reconstruction and range information from an FM-chirp waveform.

3.2 The Experiment

Figure 4 illustrates our SA system geometry. The illumination source was a New Focus 6328HP external-cavity single-mode tunable laser with approximately 5 mW of power at 1.55 μm, measured at the fiber output from the laser. The frequency was varied with a tilting-mirror/grating combination, providing a linear wavelength sweep of 10 nm in 1 second. Ninety percent of the light was used for the target interferometer, while 10% was used for the reference interferometer and HCN cell. The target beam was propagated through a length of single mode fiber containing a circulator. To form a heterodyne detection system, the 4% reflection from the end of the fiber was used as the LO. The divergent, diffraction-limited beam at the output of the fiber had a power of about 3 mW. A curved wave front, as required for SA processing, illuminated the target. A lens with a focal length of 8 cm reduced the curvature of the beam at the target, while keeping the size of the beam ≈ 1 cm. This arrangement allows simulation of longer diffraction distances with shorter working distances for convenience in the laboratory. For our experiment, this setup simulated an effective aperture of about 150 μm, at 1 m range. The actual target range was 30 cm. The target, a photograph of which is shown in Fig. 5, consisted of the letters "**NRL**" cut out from reflecting tape and mounted on an aluminum plate at a 45-degree angle of incidence in the Y direction (perpendicular to the simulated direction of flight) to allow oblique illumination. Flight was simulated by translating the target in the X direction in 50 μm increments with a computer-controlled translation stage. This allows each target point to sample different parts of the curved wave front, thereby generating a full phase history. The laser was scanned in wavelength over a span of 10 nm at each X position. Light backscattered from the target was collected by the lens and returned to the transmitting fiber. The fiber-optic circulator directed the light that entered the fiber, along with the LO light, to the InGaAs photodiode detector. The resulting heterodyne signal was digitized and stored on a computer for processing. To acquire a 1×1 cm image, 200 frequency sweeps with one sweep per 50 μm step were performed. Acquisition of a complete image required a total of 6 minutes.

Image information in the Y (= range) direction is determined from the beat frequency between the return signal and the LO. To obtain 2-D information, both the amplitude and the phase of the heterodyne signal were digitized and stored. The amplitude of the beat frequency is used to assign brightness to the derived position in the final image. Spatial resolution in the Y direction is determined by the total frequency range of the chirp waveform and is independent of range. The heterodyne signal I_H for a linear frequency chirp is given by [cf. Eq. (3) of Section 2.1]

$$I_H(t) \propto E_L E_S \cos\left(2\pi \times 2\dot{f}\,\frac{\Delta z_S}{c}\,t + \varphi_S \right), \tag{29}$$

where E_L and E_S are the local oscillator and signal fields, respectively, $\dot{f} = \Delta f_{ch}/\tau_{pul}$ is the chirp rate resulting from sweeping the laser through the frequency range Δf_{ch} in the pulse time τ_{pul}, Δz_S is the distance between the end of the fiber and a resolved spot on the sample, c is the speed of light, t is time, and φ_S is an arbitrary phase . Observe that the time delay between the LO and the light returned from the scene is $\Delta t = 2\Delta z_S/c$.
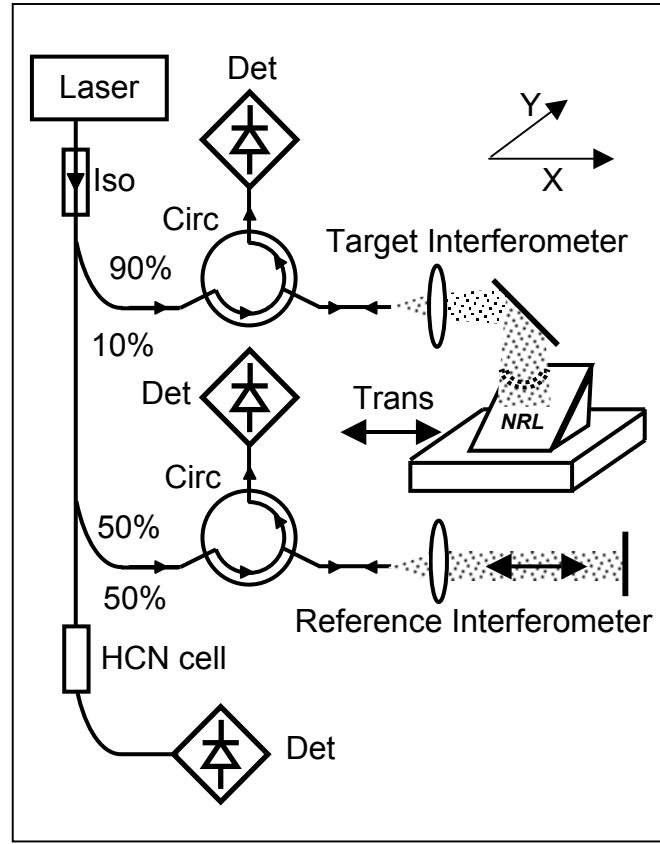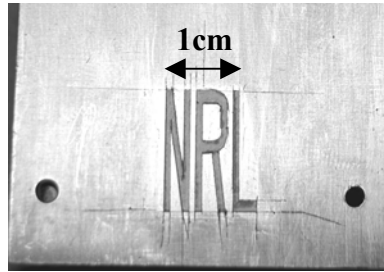
Laser

Det

Iso

Circ

90%

10%

Det

Circ

50%

50%

HCN cell

Det

Y

X

Target Interferometer

Trans

NRL

Reference Interferometer

Fig. 4 — Experimental setup

1cm

NRL

Fig. 5 — The target: **NRL** in reflective
tape on aluminum plate

The heterodyne beat frequency in Eq. (29) is $v_H = \dot{f} \Delta t = \dot{f} \, 2\Delta z_S/c = (2\Delta z_S/\lambda^2)(d\lambda/dt)$, where λ is the instantaneous wavelength and $df = (c/\lambda^2)d\lambda$ has been used. In our case, the chirp rate is 10 nm in 1 second ($\tau_{pul} = 1$ s) and $\Delta z_S = 30$ cm, so $v_H = 2.5$ kHz. With $\tau_{pul} = 1$ s, the heterodyne detector is capable of a beat frequency resolution of $1/\tau_{pul} = 1$ Hz (as explained in Section 2.1), corresponding to a range resolution of 120 μm [$\delta v_H = (2/\lambda^2)(d\lambda/dt)\delta(\Delta z_S) \Rightarrow \delta(\Delta z_S) = 120$ μm for $\delta v_H = 1$ Hz]. However, before correction, resolution is much worse, partly because the laser's scan is linear in wavelength, not in frequency, but mostly because the linearity of the wavelength scan is, according to the manufacturer's specification, only about 1%. In practice, we found a 32 Hz (instead of 1 Hz) beat frequency width for the return from a

point object, resulting from nonlinearities over the 10-nm wavelength scan. To overcome this factor-of-32 loss of resolution, we sent $\approx$ 5% of the light into a reference interferometer, as shown in Fig. 4, with $\Delta z_R \approx \Delta z_S$ + 1 cm. In the reference interferometer, the object is a flat mirror perpendicular to the beam, so there is only one range element. Therefore, variations in the heterodyne beat frequency can be due only to scan nonlinearity, so the reference interferometer can be used to monitor scan non-linearity and correct its effects. This device would not be needed in an operational system using a highly stabilized laser. When the signals in the target and reference interferometers are multiplied together and passed through a low-pass filter (i.e., double-heterodyned; this is done digitally in the computer) only the beat frequency variations caused by different ranges remain in the signal, which is the same as Eq. (29) but with the range Δz_S replaced by the range difference $\Delta z_D = \Delta z_S - \Delta z_R$:

$$I'_H(t) \propto E_L E_S \cos\left(2\pi \times 2\dot{f}\,\frac{\Delta z_D}{c}\,t + \varphi_S \right). \tag{30}$$

For our system, $\Delta z_D \leq 1$ cm. The heterodyne frequency under these conditions is reduced to 83 Hz with the error due to chirp nonlinearity being essentially eliminated. Since the sample is at $\approx$ 45-degree angle of incidence, the resolution in the target plane is decreased by a factor of 1.4. The resolution in the Y direction projected on the target is thus $120 \times 1.4 = 170$ μm.

In order to prevent random phase fluctuations due to air currents during data collection, the experiment was done in an enclosed section on a floating optical table. Small variations in the starting wavelength of different wavelength sweeps can produce artifacts in the phase history that corrupt SA image generation. Therefore, SAL 2-D imaging requires control of the laser wavelength at the start of each scan to a highly reproducible value. For SA processing to work, the resulting phase fluctuations need to be substantially smaller than 2π. In the 1.55 μm range, HCN has a number of very narrow absorption lines. About 5% of the light from the laser was sent through an HCN cell and data collection is triggered by the sudden change in transmission from one of these lines. The resulting starting frequency is reproducible to about 0.01 nm, thereby providing scan-to-scan phase coherence much better than one radian.

Image information along the X direction is provided by analysis of the stored phase values for each Y position, as discussed in detail in Section 2.3. As the curved wave front of the diffraction-limited laser beam crosses each spot of the target, a unique phase signature is generated during the heterodyne detection. Analysis of the phase data yields the X position from the unique phase signature. The best theoretical resolution in the X direction is equal to ½ the diameter of the transmitting aperture and is range independent [21; see also Eq. (B5)]. For our system this corresponds to 75 μm (= ½ the diameter of the 150 μm effective aperture). The 1 cm beam diameter at the target is diffraction-limited by the size of the effective aperture and is therefore the resolution the system would have without SA processing. In this case SA processing improves resolution by a factor of more than 100: (1 cm)/(75 μm) = 133. To retrieve the image from the data that were stored on a computer, standard SA processing was carried out, as explained in Section 2.3.

Figure 6 shows the raw data before SA processing, with 200×200 points showing the real part of the Fourier transform of I'_H along the Y axis, as a function of X position. The frequency varies from 0 to 200 Hz. The phase information is spread out over the length of the picture. Figure 7 shows the result of SA processing. Since the target was slightly longer than 1 cm in the X direction, two SAL images, overlapping by 5 mm, were combined to create the figure. As part of SA processing, we also compensated for the laser beam's Gaussian profile (cf. Section 2.3). As expected for coherent detection, the image consists of speckles. The X and Y resolution in the image, estimated from the speckle size, is about 90 μm by 170 μm, in good agreement with the predicted 75-μm by 170-μm resolution of SA processing.
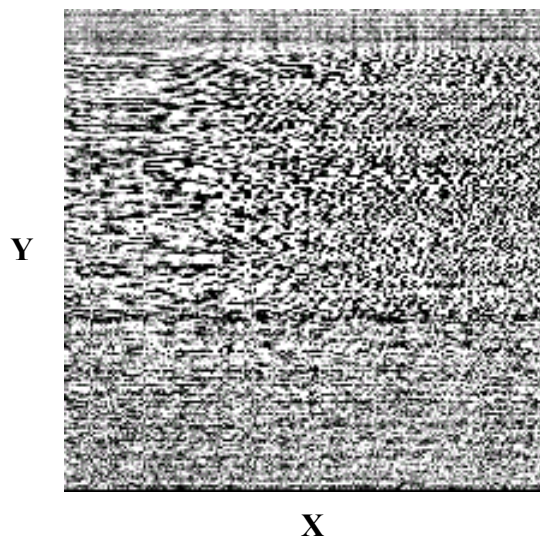
Fig. 6 — Real part of the Fourier transform of the raw
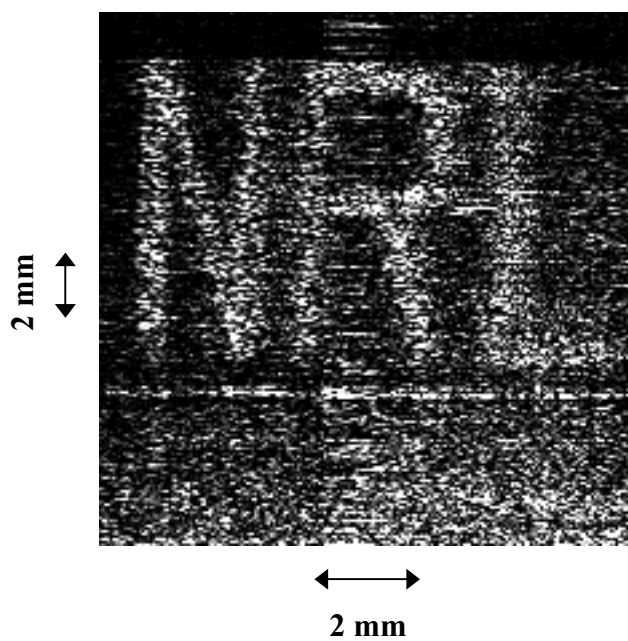data, before SAL processing

Fig. 7 — Processed image of the target shown in Fig. 5.
Vertical direction is the projected range Y and
horizontal direction is X.

4. SUMMARY

This report argues the theoretical feasibility of an orbit-based SAL at IR wavelengths for achieving centimeter-class resolution, an argument backed up by the first laboratory demonstration of 2-D imaging with a scan-mode SAL. The relatively restricted set of observation ranges appropriate for an operational SAL, a few hundred to several thousand kilometers, is suited to the orbit-based surveillance problem. At shorter ranges, conventional imaging in visible light can provide high resolution, at longer ranges, excessive laser power and/or real collecting aperture size is required. SAL's limitations of low SNR and area coverage for single-look imagery can be alleviated by multiple images and mosaicking of scenes.

The effect of photon counting statistics on SNR for SAL has been developed. Equations (13) and (14) show that a low photon rate imposes a much greater SNR penalty on SAL than on a direct detection system. For SAL, if laser power and receiving aperture are not high enough to produce an SNR close to ½ in single-look imagery, then, compared to direct detection, a much larger number of repeated images must be combined to achieve an SNR approaching unity. (But direct detection requires a much bigger real aperture to achieve the same resolution.)

Various engineering difficulties have been touched upon in the course of the discussion. The most obvious are the laser technology issues of developing high-power, space-qualified lasers with fast chirp rates, pulse repetition frequencies of tens or hundreds of kilohertz, and coherence times up to tens or even hundreds of milliseconds. Another major engineering problem is providing line-of-sight pointing control consistent with the desired footprint size and capable of executing multiple scans of the scene in order to produce some combination of increased SNR, increased area coverage, increased resolution, and reduced laser power. As stated in Section 2.3, generating the matched filter coefficients for SA signal processing requires compensating for platform vibrations to an accuracy better than the wavelength of the light used, a problem that requires sensitive accelerometers but will be easier to deal with for the smooth motion of a spacecraft than for an airborne system. To an extent, this problem can be handled in post-processing by the focusing methods developed for SAR. Yet another problem is the need to place many heterodyne detectors in the receiver focal plane when $D_R > D_T$.

AKNOWLEDGMENT

REFERENCES

1. T.J. Green, S. Marcus, and B.D. Colella, "Synthetic-aperture-radar Imaging with a Solid-state Laser," *Ap. Opt.* **34**(30), 6,941 – 6,949, 1995.

2. S. Yoshikado and T. Aruga, "Short-Range Verification Experiment of a Trial One-Dimensional Synthetic Aperture Infrared Laser Radar Operated in the 10 µ Band," *Ap. Opt.* **39**(9), 1,421 – 1,425, 2000.

3. R.L. Lucke and L.J Rickard, "Photon-Limited Synthetic-Aperture Imaging for Planet Surface Studies," *Ap. Opt.* **41**(24), 5,084 – 5,095, 2002.

4. J.C. Curlander and R.N. McDonough, *Synthetic Aperture Radar: Systems and Signal Processing* (John Wiley & Sons, New York, 1991).

5. C.V. Jakowatz, D.E. Wahl, P.H. Eichel, D.C. Ghiglia, and P.A. Thompson, *Spotlight-Mode Synthetic Aperture Radar: A Signal Processing Approach* (Kluwer Academic Publishers, Boston, 1996).

6. M. Bashkansky, R.L. Lucke, E. Funk, J. Reintjes, "Two-Dimensional Synthetic-Aperture Imaging in the Optical Domain," *Opt. Lett.* **27**(22), 1,983-1,985, 2002.

7. J.H. Shapiro, B.A. Capron, and R.C. Harney, "Imaging and Target Detection with a Heterodyne-Reception Optical Radar," *Ap. Opt.* **20**(19), 3,292 – 3,313, 1981.

8. D. Park and J.H. Shapiro, "Performance Analysis of Optical Synthetic Aperture Radars," *SPIE* **99**, *Laser Radar II*, 100 – 116, 1988.

9. T.G. Kyle, "High Resolution Laser Imaging System," *Ap. Opt.* **28**(13), 2,651 – 2,656, 1989.

10. C.C. Aleksoff, J.S. Accetta, L.M. Peterson, A.M. Thai, A. Kooster, K.S. Schroeder, R.M. Majewski, J.O. Abshier, and M. Fee, "Synthetic Aperture Imaging with a Pulsed CO_2 TEA Laser," *SPIE* **783**, *Laser Radar II*, 29 – 40, 1987.

11. R.H. Kingston, *Detection of Optical and Infrared Radiation* (Springer-Verlag, New York, 1978), p. 27.

12. P.J. Winzer and W.R. Leeb, "Coherent Lidar at Low Signal Powers: Basic Considerations on Optical Heterodyning," *J. Mod. Opt.* **45**(8), 1,549 – 1,555, 1998.

13. J.H. Shapiro, "Target-reflectivity Theory for Coherent Laser Radars," *Ap. Opt.* **21**(18), 3,398 – 3,407, 1982.

14. J.W. Goodman, *Statistical Optics* (John Wiley & Sons, New York, 1985).

15. J.H. Shapiro and S.S. Wagner, "Phase and Amplitude Uncertainties in Heterodyne Detection," *IEEE J. Quant. Elec.* **QE-20**(7), 803 – 813, 1984.

16. R. Loudon, *The Quantum Theory of Light* (Clarendon Press, Oxford, 1983), Section 4.8.

17. M.C. Amann, T. Bosch, M. Lescure, R. Myllylä, and M. Rioux, "Laser Ranging: a Critical Review of Usual Techniques for Distance Measurement," *Opt. Eng.* **40**, 10, 2001.

18. R. Schneider, P. Thurmel, and M. Stockman, "Distance Measurement of Moving Objects by Frequency Modulated Laser Radar," *Opt. Eng.* **40**, 33, 2001.

19. S. Markus, B.D. Colella, and T.J. Green, Jr., "Solid-state Laser Synthetic Aperture Radar," *Appl. Opt.* **33**, 960, 1994.

20. A.B. Geschwendtner and W.E. Keicher, "Development of Coherent Laser Radar at Lincoln Laboratory," *Lincoln Lab. J.* **12**, 383, 2000.

21. L.J. Cutrona, in *Radar Handbook*, M.I. Skolnik, ed. (McGraw Hill, New York, 1970).

Appendix A

TWO-DIMENSIONAL GAUSSIAN PROBABILITY

Following Goodman,[*] a complex number, $a\exp(i\theta)$, is called a phasor. Goodman calculates the two-dimensional probability density function that describes the sum of a large number of random phasors. There are two points in this paper to which this PDF is relevant: finding (1) the frequency content of shot noise and the consequent variance with which a detected number of photons is measured by heterodyne detection, and (2) how contributions from the pixels in the beam's ground footprint add up to make the measured signal. In both cases we need to know the sum of N of these random phasors. The sum is an origin-centered 2-D Gaussian distribution described by $\sigma^2 = N\langle a^2\rangle/2$, where $\langle a^2\rangle$ is the expectation value of a^2 over the distribution from which a is chosen, and phase is assumed random and uniformly distributed over $(-\pi, \pi)$. Adding a complex value s, representing a signal, to this distribution displaces its center a distance $|s|$ from the origin, and we may, without loss of generality, take s to be real and non-negative, so the PDF of the sum plus signal is

$$P(x, y) = \frac{1}{2\pi\sigma^2}\exp\left[-\frac{(x-s)^2 + y^2}{2\sigma^2}\right], \tag{A1}$$

which is taken from Goodman's Eq. (2.9-18) with minor changes in notation. x and y represent the real and imaginary parts, respectively, of a complex number. In extension of the definition of variance for a 1-D Gaussian distribution, the variance of this PDF is

$$\mathrm{Var}\left[P(x, y)\right] \equiv \left\langle (x-s)^2 + y^2\right\rangle = \left\langle (x-s)^2\right\rangle + \left\langle y^2\right\rangle = 2\sigma^2. \tag{A2}$$

When $s = 0$, $(2\sigma^2)^{1/2} = N^{1/2}a_{\mathrm{rms}}$ is the rms value of the magnitude of the sum.

The value of σ^2 for heterodyne detection is found by evaluating shot noise. The easiest way to see that shot noise results in white, Gaussian noise in frequency space is to write the current produced in a detector of quantum efficiency η_d by N impinging photons as

$$I(t) = \sum_{n=1}^{\eta_d N} q_e\delta\left(t - t_n\right), \tag{A3}$$

where q_e is the electronic charge, the sum is over the $\eta_d N$ detected photons, and t_n is the creation time of the nth electron. The Fourier transform of this current is

---

[*]   J.W. Goodman, *Statistical Optics* (John Wiley & Sons, New York, 1985).

$$\text{FT}\big[I(t)\big] = \int_0^T \sum_{n=1}^{\eta_d N} q_e \delta\big(t - t_n\big) \exp\big(-2\pi i f t\big) \, dt$$

$$= \sum_{n=1}^{\eta_d N} q_e \exp\big(-2\pi i f t_n\big) \quad . \tag{A4}$$

Since the t_n are randomly distributed, the second sum in Eq. (A4) is the sum of a large number of phasors with (constant) amplitude q_e and random phase $2\pi f t_n$. Therefore, independently of f, the result is an origin-centered 2-D Gaussian distribution described by Eq. (A1) with $s = 0$ and

$$\sigma^2 = q_e^2 \eta_d N / 2 \quad . \tag{A5}$$

A random number chosen from this distribution is the noise that is added to the DFT component shown in Eq. (4), and, divided by $(q_e \eta_d)^2 \eta_h N_L$, appears as the noise term E_m in Table 1.

Equation (A4) uses the continuous Fourier transform as an easy way to reach the desired result. If the idealized response $\delta(t - t_n)$ is replaced by the actual detector response having finite width, and this width is reasonably densely sampled, the same result is obtained with the discrete Fourier transform used in Eq. (4). The reader who wishes to pursue this topic further may consult Lucke[*] where the properties of photon-limited noise in the DFT of spatial data are explicated at length. The discussion there applies also to the DFT of temporal data, and that paper's Eq. (26) is the equivalent of Eq. (A5) once it is recognized that the total number of photons detected is closely approximated by $\eta_d N_L$ and that the error figure shown in this paper's Fig. 1 is circular (so that, as described in the other paper, $S_{2k} = 0$).

---

[*]   R.L. Lucke, "Fourier-space Properties of Photon-Limited Noise in Focal Plane Array Data, Calculated with the Discrete Fourier Transform," *J. Opt. Soc. Am. A* **18**(4), 777 – 790, 2001.

Appendix B

SYNTHETIC APERTURE PROCESSING AND RESOLUTION

The pixel 0 column of Table 1 shows that the matched filter gives a value of MA_0 for the desired pixel. To justify the claim that the other pixels add to "≈ 0", we first examine the pixel 1 column, which is

$$\sum_{m=1}^{M-1} A_1 C_m C_{m-1}^* = A_1 \sum_{m=1}^{M-1} \exp\left\{i\frac{2\pi p^2}{\lambda R}\left[\left(m - \frac{M}{2}\right)^2 - \left(m - 1 - \frac{M}{2}\right)^2\right]\right\}$$
$$= A_1 \sum_{m=1}^{M-1} \exp\left\{i\frac{4\pi p^2}{\lambda R}\left(m - \frac{M+1}{2}\right)\right\} , \tag{B1}$$

where $C_m = \exp\{2\pi i[(m - M/2)p]^2/\lambda R\}$ has been used. The sum on the right side of the second equality is the sum of $M - 1$ unit-amplitude phasors with phase increment $\Delta\phi = 4\pi p^2/\lambda R$. The sum is exactly zero – the phasors "wrap" to zero – if the phase of the last phasor is $2\pi - \Delta\phi$ greater than the phase of the first, i.e., if

$$\frac{4\pi p^2}{\lambda R}\left[\left(M - 1 - \frac{M+1}{2}\right) - \left(1 - \frac{M+1}{2}\right)\right] = \frac{4\pi p^2}{\lambda R}(M - 2) = 2\pi - \frac{4\pi p^2}{\lambda R} , \tag{B2}$$

or

$$\frac{4\pi M p^2}{\lambda R}\left(1 - \frac{1}{M}\right) = 2\pi , \tag{B3}$$

whence

$$p = \frac{\lambda R}{2F}, \tag{B4}$$

where $F = Mp$ is the size of the illuminated footprint and $M \gg 1$ has been used. Further, if F is determined by the diffraction-limited resolution of a transmitting aperture with diameter D_T, i.e., $F = \lambda R/D_T$, we find

$$p = \frac{D_T}{2}, \tag{B5}$$

for the resolution of an SA system. Equation (B5) is the same as, for example, Eq. (1.2.9) of Curlander and McDonough.[*]

---

[*] J.C. Curlander and R.N. McDonough, *Synthetic Aperture Radar: Systems and Signal Processing* (John Wiley & Sons, New York, 1991).

Equations (B1) through (B3) are exact only if pixel 1 consists of a point object at its center. Since the return is actually spread out over the pixel, these equations are approximate, but the basic principle remains: the pixel 1 column of Table 1 makes only a small contribution to the last row because the phasors wrap to (nearly) zero. In the pixel 2 column, the phase increment is twice as big and the wrapping happens faster. The pixel M - 1 column makes a small contribution because it contains only a single term. Intermediate columns make small contributions by a combination of these effects. Finally, all these small contributions are random phasors that add up across the bottom row of the table to give a sum that is small compared to the coherent sum, MA_0, from pixel 0.